

# PUSHING BISTATIC WIRELESS SENSING TOWARD HIGH ACCURACY AT THE SUB-WAVELENGTH SCALE

Wenwei Li<sup>†</sup>    Jiarun Zhou<sup>†</sup>    Qinxiao Quan<sup>†</sup>    Fusang Zhang<sup>‡</sup>    Daqing Zhang<sup>†\*</sup>

<sup>†</sup>School of Computer Science, Peking University, Beijing, China

<sup>‡</sup>School of Cyber Science and Technology, Beihang University, Beijing, China

\*Telecom SudParis, Institut Polytechnique de Paris, Paris, France

## ABSTRACT

Contactless sensing using wireless communication signals has garnered significant attention due to its non-intrusive nature and ubiquitous infrastructure. Despite the promise, the inherent bistatic deployment of wireless communication introduces clock asynchronism, which leads to unknown phase offsets in channel response and hinders fine-grained sensing. State-of-the-art systems widely adopt the cross-antenna channel ratio to cancel these detrimental phase offsets. However, the channel ratio preserves sensing feature accuracy only at integer-wavelength target displacements, losing sub-wavelength fidelity. To overcome this limitation, we derive the first quantitative mapping between the distorted ratio feature and the ideal channel feature. Building on this foundation, we develop a robust framework that leverages channel response amplitude to recover the ideal channel feature from the distorted ratio. Real-world experiments across Wi-Fi and LoRa demonstrate that our method can effectively reconstruct sub-wavelength displacement details, achieving nearly an order-of-magnitude improvement in accuracy.

**Index Terms**— Contactless Sensing, Bistatic Wireless System, Channel Ratio, Integrated Sensing and Communication

## 1. INTRODUCTION

Alongside the rapid proliferation of commodity wireless communication, contactless sensing leveraging ubiquitous wireless signals has attracted widespread attention over the past decade. Compared with traditional sensing modalities that rely on dedicated sensors, wearables, or cameras, this emerging paradigm offers compelling advantages in terms of low cost, non-intrusiveness, and privacy preservation. A wide range of signals, including Wi-Fi, 4G/5G cellular networks, and LoRa, have been explored for contactless sensing, enabling key applications such as vital sign monitoring [1, 2], activity recognition [3, 4], and device-free tracking [5, 6].

While wireless communication systems hold great promise for sensing applications, their inherent bistatic deployment introduces a fundamental issue of clock asynchronism. Specifically, the spatially separated transmitter and receiver typically operate on two independent oscillators, resulting in mismatches such as Carrier Frequency Offset (CFO) and Sampling Frequency Offset (SFO) between the two ends [7, 8]. These mismatches induce unknown time-varying phase offsets in the channel response measurements, which obscure

the true channel phase changes induced by target motions. Under these detrimental phase offsets, only amplitude information remains usable for sensing, significantly limiting the precision and range of potential applications [1, 9].

Prior studies have investigated various approaches to recover clean channel phase measurements for fine-grained sensing. Early works [10, 11, 12, 13] employed channel correlations to estimate and reduce detrimental phase offsets, but residual offsets from estimation bias can still compromise phase accuracy. Later efforts leveraged the cross-antenna consistency of these offsets. Some systems [14, 15, 16, 17] employed the cross-antenna conjugate multiplication of channel measurements to cancel the offsets, but this approach suffers from spurious motion components [18] and low SNR [9]. In contrast, state-of-the-art systems [1, 2, 9, 18, 4, 19, 20], spanning Wi-Fi, 4G/5G, and LoRa, have widely adopted the cross-antenna channel ratio, which cancels the phase offsets while largely preserving the sensing properties of the ideal channel response. However, although the channel ratio provides sensing features fully consistent with the ideal channel response when the target displacement is exactly an integer multiple of the wavelength, discrepancies arise at the sub-wavelength scale. For instance, with 2.4 GHz Wi-Fi signals of 12 cm wavelength, the channel ratio can inherently introduce sensing errors of up to 6 cm during continuous target displacements. For signals with longer wavelengths, such as LoRa, these ratio-induced errors become even more significant. Therefore, existing systems still face challenges in achieving high accuracy at the sub-wavelength scale.

In this paper, we present a novel framework to reconstruct sub-wavelength accuracy from the channel ratio. To this end, we move beyond the prior qualitative understanding of the channel ratio and derive the first quantitative mapping that models the sub-wavelength feature distortion induced by the channel ratio. Notably, we reveal that this mapping is determined only by channel response amplitude, which is unaffected by detrimental phase offsets. Building on this model, we design a robust pipeline that leverages the amplitude of channel measurements to recover the ideal sensing feature from the distorted channel ratio feature. To validate our framework, we conduct real-world experiments using both Wi-Fi and LoRa signals. The results show that our framework reduces the displacement estimation error of the state-of-the-art method by nearly an order of magnitude, achieving high accuracy at the sub-wavelength scale.

The rest of the paper is organized as follows. Section 2 introduces the basics of bistatic wireless sensing and the channel ratio. Section 3 presents the proposed model and framework. Section 4 reports experimental results, and Section 5 concludes the paper.

Corresponding author: Daqing Zhang. This work is supported by the National Science and Technology Major Project (Grant No. 2025ZD1302100).

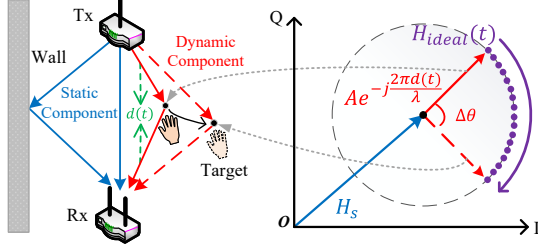


Fig. 1. Illustration of ideal channel responses.

## 2. PRELIMINARY

### 2.1. Bistatic Wireless Sensing

In typical wireless communication environments, signals propagate from the transmitter to the receiver along multiple paths. By comparing the received signal with the known transmitted signal (e.g., preamble in Wi-Fi/4G/5G and dechirped symbol in LoRa), the receiver can estimate the channel response within the band of interest. As a superposition of components from all paths, the ideal channel response  $H_{\text{ideal}}(t)$  can be expressed as

$$H_{\text{ideal}}(t) = \sum_i a_i e^{-j\frac{2\pi d_i(t)}{\lambda}} = H_s + Ae^{-j\frac{2\pi d(t)}{\lambda}}, \quad (1)$$

where  $a_i$ ,  $e^{-j\frac{2\pi d_i(t)}{\lambda}}$ , and  $d_i$  are the attenuation, phase shift, and path length of the  $i$ -th path signal, respectively, and  $\lambda$  is the wavelength. When a target moves within the propagation environment, the channel response can be decomposed into a static component  $H_s$ , resulting from the direct path and reflections from stationary objects, and a dynamic component  $Ae^{-j\frac{2\pi d(t)}{\lambda}}$ , contributed by the reflection from the moving target. As target motions cause the reflection path length  $d(t)$  to change, the channel response vector rotates along a circle, as shown in Figure 1. The key principle of fine-grained sensing is to extract the angle of this rotation, i.e., the dynamic phase change  $\Delta\theta = -\frac{2\pi\Delta d}{\lambda}$ , thereby quantifying the path length change  $\Delta d$  and the target displacement.

In practical bistatic systems, clock asynchronism between transmitter and receiver introduces mismatches such as CFO and SFO. As a result, the actual channel response measurement  $H(t)$  is impacted by an unknown time-varying phase offset  $\phi_{\text{offset}}(t)$  and can be expressed as

$$H(t) = e^{-j\phi_{\text{offset}}(t)} \left( H_s + Ae^{-j\frac{2\pi d(t)}{\lambda}} \right). \quad (2)$$

This detrimental phase offset varies significantly and obscures the phase change caused by target motions [9, 21], making it challenging in practice to extract the rotation angle  $\Delta\theta$  for fine-grained sensing.

### 2.2. Cross-Antenna Channel Ratio

To recover a clean channel response phase, state-of-the-art systems widely employ the cross-antenna channel ratio technique. The underlying principle of this method is that multiple antennas on a single receiver typically share a common oscillator. Therefore, the phase offset induced by clock asynchronism is identical across receiver antennas. By computing the ratio of channel measurements from

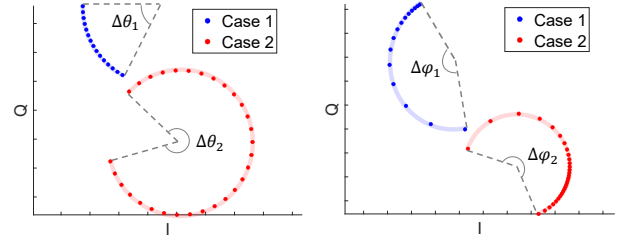


Fig. 2. The rotation feature of the channel ratio is distorted under sub-wavelength-scale variations.

two antennas, the detrimental phase offset can be perfectly canceled. Specifically, the channel ratio  $H_{\text{ratio}}(t)$  can be expressed as

$$\begin{aligned} H_{\text{ratio}}(t) &= \frac{H_1(t)}{H_2(t)} = \frac{e^{-j\phi_{\text{offset}}(t)} \left( H_{s,1} + A_1 e^{-j\frac{2\pi d_1(t)}{\lambda}} \right)}{e^{-j\phi_{\text{offset}}(t)} \left( H_{s,2} + A_2 e^{-j\frac{2\pi d_2(t)}{\lambda}} \right)} \\ &= \frac{H_{s,1} + \widetilde{A}_1 e^{-j\frac{2\pi d_2(t)}{\lambda}}}{H_{s,2} + A_2 e^{-j\frac{2\pi d_2(t)}{\lambda}}} = \frac{\mathcal{A}z(t) + \mathcal{B}}{\mathcal{C}z(t) + \mathcal{D}}, \end{aligned}$$

where  $A_{(1,2)}$  and  $e^{-j\frac{2\pi d_{(1,2)}(t)}{\lambda}}$  represent the amplitude and phase of the dynamic channel components at two different antennas, respectively, and  $\widetilde{A}_1 = A_1 e^{-j\frac{2\pi(d_1-d_2)}{\lambda}}$  can be regarded as a constant over a short period [1, 9]. In this form, the channel ratio can be viewed as a Möbius transformation [22] of  $z(t) = e^{-j\frac{2\pi d_2(t)}{\lambda}}$ .

A key property of the Möbius transformation is its preservation of circularity [22]. Since  $z(t)$  traces the unit circle, the channel ratio also traces a circle. More importantly, when  $z(t)$  rotates one full cycle of  $2\pi$  (i.e., the target path length changes by one wavelength), the channel ratio also rotates exactly one full cycle, consistent with the ideal channel response. This property enables us to accurately estimate the path length change  $\Delta d$  at the integer-wavelength scale by extracting the rotation angle of the channel ratio.

Although the channel ratio enables accurate sensing at the integer-wavelength scale, it loses accuracy at the sub-wavelength scale. As shown in Figure 2, when the path length change  $\Delta d$  is not an integer multiple of the wavelength, the rotation angle of the channel ratio may deviate significantly from that of the ideal channel response. This deviation fundamentally limits the capability of channel-ratio-based methods to achieve sub-wavelength accuracy.

## 3. METHOD

In this section, we first establish a quantitative mapping between the rotation angle of the channel ratio and that of the ideal channel response. Based on this model, we propose a framework that leverages the amplitude of raw channel measurements to recover the rotation angle of the ideal channel response from the distorted channel ratio.

### 3.1. Modeling the Rotation Angle of the Channel Ratio

As the channel ratio traces a circle in the complex plane, it can be expressed as

$$H_{\text{ratio}} = \frac{H_{s,1} + \widetilde{A}_1 e^{j\theta}}{H_{s,2} + A_2 e^{j\theta}} = H_{s,\text{ratio}} + A_{\text{ratio}} e^{j\varphi}, \quad (3)$$

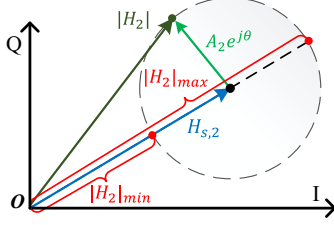


**Fig. 3.** Illustration of  $|H_2|_{\max}$  and  $|H_2|_{\min}$ .

where  $H_{s,\text{ratio}}$  and  $A_{\text{ratio}}$  denote the center and the radius of the circle, respectively,  $\varphi$  denote the angle of the channel ratio on the circle, and  $\theta$  denotes  $-\frac{2\pi d_2(t)}{\lambda}$ . Under these definitions,  $\Delta\varphi$  is the rotation angle of the channel ratio, while  $\Delta\theta$  is the rotation angle of the ideal channel response.

To model the rotation angle of the channel ratio, we analyze the variation of the channel ratio during the rotation. We assume that the variations under analysis are sufficiently small (*e.g.*, between two adjacent samples), which allows us to employ differential approximation to facilitate our analysis. Larger variations can be derived by accumulating such small variations. Based on the circle-trace expression in Equation 3, the magnitude of the channel ratio variations can be expressed as

$$|\Delta H_{\text{ratio}}| = \left| \Delta(H_{s,\text{ratio}} + A_{\text{ratio}}e^{j\varphi}) \right| \approx A_{\text{ratio}}\Delta\varphi. \quad (4)$$

On the other hand, as the variation of the ratio of two channel responses, its magnitude can also be expressed as

$$\begin{aligned} |\Delta H_{\text{ratio}}| &= \left| \Delta \left( \frac{H_{s,1} + \widetilde{A}_1 e^{j\theta}}{H_{s,2} + A_2 e^{j\theta}} \right) \right| \approx \frac{|\widetilde{A}_1 H_{s,2} - A_2 H_{s,1}|}{|H_{s,2} + A_2 e^{j\theta}|^2} \Delta\theta \\ &= \frac{|\widetilde{A}_1 H_{s,2} - A_2 H_{s,1}|}{|H_2|^2} \Delta\theta, \end{aligned} \quad (5)$$

where  $|H_2|$  represents the amplitude of the denominator channel measurement in the channel ratio. Note that  $|H_2|$  is unaffected by detrimental phase offsets and therefore equals the amplitude of the ideal channel response. By combining Equation 4 and 5, we can relate  $\Delta\varphi$  to  $\Delta\theta$  as

$$\Delta\varphi = \frac{\frac{1}{A_{\text{ratio}}} |\widetilde{A}_1 H_{s,2} - A_2 H_{s,1}|}{|H_2|^2} \Delta\theta = \frac{k}{|H_2|^2} \Delta\theta, \quad (6)$$

where we denote the constant term  $\frac{1}{A_{\text{ratio}}} |\widetilde{A}_1 H_{s,2} - A_2 H_{s,1}|$  as  $k$  to facilitate the subsequent analysis.

Equation 6 provides a basic mapping between  $\Delta\varphi$  and  $\Delta\theta$ . However, to reconstruct  $\Delta\theta$  from  $\Delta\varphi$ , the constant  $k$  must be expressed in terms of the accessible amplitude of channel responses. To achieve this, we exploit the property that when the channel ratio completes a full  $2\pi$  rotation, the ideal channel response also rotates exactly one full cycle. Specifically, over a  $2\pi$  rotation, the integral of the differential form on both sides of Equation 6 can be expressed as

$$\int_0^{2\pi} d\varphi = \int_0^{2\pi} \frac{k}{|H_2|^2} d\theta. \quad (7)$$

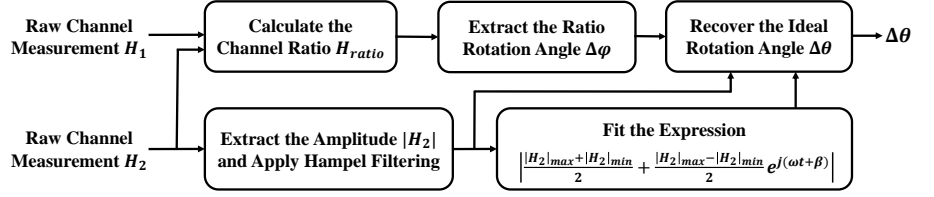


**Fig. 4.** Framework Overview.

By substituting  $|H_2|^2 = |H_{s,2} + A_2 e^{j\theta}|^2$ ,  $k$  can be calculated as

$$\begin{aligned} k &= \frac{\int_0^{2\pi} d\varphi}{\int_0^{2\pi} \frac{1}{|H_{s,2} + A_2 e^{j\theta}|^2} d\theta} = (|H_{s,2}| + A_2)(|H_{s,2}| - A_2) \\ &= |H_2|_{\max} |H_2|_{\min}, \end{aligned} \quad (8)$$

where  $|H_2|_{\max}$  and  $|H_2|_{\min}$  represent the maximum and minimum value of  $|H_2|$  during the rotation of a full cycle, as illustrated in Figure 3. Finally, we derive the mapping between  $\Delta\theta$  and  $\Delta\varphi$  as

$$\Delta\theta = \frac{|H_2|^2}{|H_2|_{\max} |H_2|_{\min}} \Delta\varphi. \quad (9)$$

Based on Equation 9, we can reconstruct  $\Delta\theta$  from  $\Delta\varphi$  by extracting  $|H_2|$ ,  $|H_2|_{\max}$  and  $|H_2|_{\min}$  from raw channel measurements.

### 3.2. Recovering the Rotation Angle of the Ideal Channel

Figure 4 presents our proposed framework for recovering the rotation angle of the ideal channel response, *i.e.*,  $\Delta\theta$ .

First, consistent with prior systems, we compute the channel ratio from the raw channel measurements of two antennas. We then employ the state-of-the-art method proposed in [3] to extract the rotation angle of the channel ratio, *i.e.*,  $\Delta\varphi$ .

Concurrently, we take the raw channel measurement that serves as the denominator of the channel ratio and extract its amplitude as  $|H_2|$ . To mitigate the impact of potential impulse noise on the channel measurement amplitude [9], we apply a Hampel filter to the raw  $|H_2|$ .

Then, we take multiple  $|H_2|$  samples within a 0.5 s time window to extract  $|H_2|_{\max}$  and  $|H_2|_{\min}$ . A naive approach of directly taking the maximum and minimum  $|H_2|$  samples as  $|H_2|_{\max}$  and  $|H_2|_{\min}$  is not robust for two reasons: (1) these extreme values are highly susceptible to outliers and noise, and (2) during small-scale target motion, the  $|H_2|$  variation may not span its full theoretical range, meaning the true maximum and minimum may not be observed. Therefore, we propose a scheme that leverages all samples within the window to estimate  $|H_2|_{\max}$  and  $|H_2|_{\min}$ . Specifically, since the channel response can be regarded as rotating uniformly within a short time window, the amplitude  $|H_2|$  can be modeled as

$$\left| \frac{|H_2|_{\max} + |H_2|_{\min}}{2} + \frac{|H_2|_{\max} - |H_2|_{\min}}{2} e^{j(\omega t + \beta)} \right|.$$

We fit this expression to multiple samples within the window using a non-linear least squares algorithm, thereby obtaining robust estimates of  $|H_2|_{\max}$  and  $|H_2|_{\min}$ .

Finally, we feed the extracted  $\Delta\varphi$ ,  $|H_2|$ ,  $|H_2|_{\max}$  and  $|H_2|_{\min}$  into Equation 9 to compute  $\Delta\theta = -2\pi\Delta d/\lambda$ . We can then quantify the path length change induced by target motion with sub-wavelength accuracy.

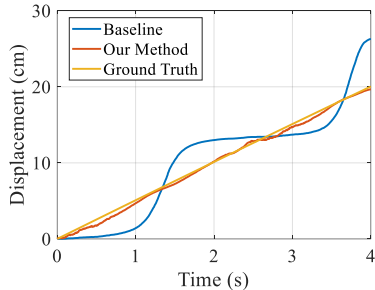


Fig. 5. Examples of displacement estimates.

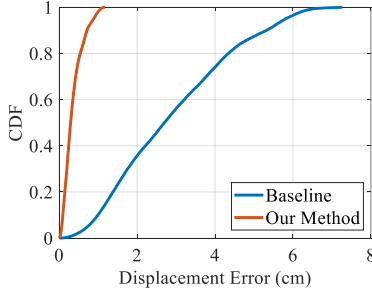


Fig. 6. Benchmark experiment results.

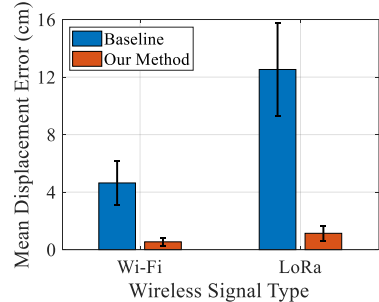


Fig. 7. Gesture experiment results.

## 4. EXPERIMENT

To evaluate our proposed framework, we conduct real-world experiments using both Wi-Fi and LoRa signals. Specifically, we evaluate the performance of our framework in estimating target displacement through a benchmark experiment and a gesture experiment.

**Wi-Fi Setup.** We use two mini PCs equipped with a commodity Intel 5300 wireless NIC to transmit and receive Wi-Fi signals. The transmitter is configured with a single antenna, while the receiver is equipped with two antennas. The Wi-Fi signals are centered at a frequency of 2.47 GHz, corresponding to a wavelength of 12.1 cm. We collect Wi-Fi Channel State Information (CSI) as channel measurements using the CSI Tool [23], at a sampling rate of 1000 Hz.

**LoRa Setup.** We use a Semtech SX1276 module with an Arduino Uno, equipped with a single antenna, as the LoRa node. The LoRa gateway is implemented using a USRP B210 equipped with two antennas and GNU Radio. The LoRa node transmits signals at a center frequency of 915 MHz, corresponding to a wavelength of 32.8 cm. We dechirp the received LoRa signals to obtain channel measurements at a sampling rate of 1000 Hz.

**Baseline.** We employ the state-of-the-art method proposed in [3] as the baseline. Our framework follows the baseline method for extracting the rotation angle of the channel ratio, but the baseline does not incorporate our sub-wavelength accuracy recovery scheme.

### 4.1. Benchmark Experiment

In the benchmark experiment, we use a  $30 \text{ cm} \times 30 \text{ cm}$  metal plate as the target. A Wi-Fi transmitter and receiver are deployed 1.2 m away from the metal plate, with a spacing of 4 m between them. The metal plate is mounted on a high-precision sliding track with a digital controller, enabling displacement control with an accuracy of 1 mm. We configure the metal plate to move along the perpendicular bisector of the transceiver pair at speeds of 1 cm/s, 2 cm/s, and 5 cm/s, with displacement distances of 2 cm, 5 cm, 10 cm, 15 cm, and 20 cm. Each experiment is repeated 20 times.

Figure 5 shows an example of displacement estimation results over time for a single target movement experiment. We observe that when the target path length change is not an exact integer multiple of the wavelength, the baseline method exhibits periodic over- or under-estimation relative to the sliding track ground truth, with a maximum error of 6.3 cm. In contrast, our method maintains displacement estimates consistent with the ground truth at the sub-wavelength scale, with a maximum error below 0.9 cm.

Figure 6 presents the Cumulative Distribution Functions (CDFs)

of displacement estimation errors across all benchmark experiments. It can be observed that our method reduces the median error from 2.7 cm to 0.3 cm, and the 90th-percentile error from 5.3 cm to 0.7 cm. These results demonstrate that our framework significantly advances the sensing accuracy limits at the sub-wavelength scale.

### 4.2. Quantifying Gesture Displacement

To evaluate the potential of our framework in sensing applications, we conduct gesture experiments using both Wi-Fi and LoRa devices. In these experiments, the transmitter and receiver are placed on a table in an office environment, separated by 2 m. Volunteers perform gestures from an initial position 1 m away from the transceivers. To obtain the ground truth, we pre-mark reference points on the table at displacements of 5 cm, 10 cm, 15 cm, and 20 cm, and instruct the volunteers to move their hands between these points. We recruit four volunteers (two males and two females) to participate in the experiments, and each experiment is repeated 10 times.

Figure 7 presents the average displacement estimation errors of our method compared with the baseline. Notably, our method achieves nearly an order-of-magnitude improvement in accuracy for both Wi-Fi and LoRa sensing. Specifically, when sensing with Wi-Fi signals, the average errors of the baseline and our framework are 4.6 cm and 0.5 cm, respectively. When using LoRa signals, which have a longer wavelength, the average error of the baseline increases to 12.5 cm, while our method maintains a low average error of 1.1 cm. These results demonstrate that our framework significantly enhances the sub-wavelength accuracy of gesture displacement estimation, opening new opportunities such as fine-grained control of IoT devices via in-air gestures.

## 5. CONCLUSION

In this paper, we address the fundamental sub-wavelength accuracy limitation in bistatic wireless sensing based on the channel ratio. Beyond prior qualitative understanding, we derive the first quantitative mapping between the distorted sensing feature of the channel ratio and the ideal sensing feature. We reveal that this mapping is determined only by the amplitude of channel responses, which is unaffected by detrimental phase offsets in bistatic wireless systems. Building on this foundation, we propose a robust framework to recover the ideal sensing feature from the distorted channel ratio. Real-world experiments across Wi-Fi and LoRa demonstrate that our framework achieves nearly an order-of-magnitude accuracy improvement at the sub-wavelength scale.

## 6. REFERENCES

- [1] Youwei Zeng, Dan Wu, Jie Xiong, Enze Yi, Ruiyang Gao, and Daqing Zhang, “Farsense: Pushing the range limit of wifi-based respiration sensing with csi ratio of two antennas,” *Proceedings of the ACM on Interactive, Mobile, Wearable and Ubiquitous Technologies*, vol. 3, no. 3, pp. 1–26, 2019.
- [2] Fusang Zhang, Zhaoxin Chang, Jie Xiong, Rong Zheng, Junqi Ma, Kai Niu, Beihong Jin, and Daqing Zhang, “Unlocking the beamforming potential of lora for long-range multi-target respiration sensing,” *Proceedings of the ACM on Interactive, Mobile, Wearable and Ubiquitous Technologies*, vol. 5, no. 2, pp. 1–25, 2021.
- [3] Ruiyang Gao, Wenwei Li, Yaxiong Xie, Enze Yi, Leye Wang, Dan Wu, and Daqing Zhang, “Towards robust gesture recognition by characterizing the sensing quality of wifi signals,” *Proceedings of the ACM on Interactive, Mobile, Wearable and Ubiquitous Technologies*, vol. 6, no. 1, pp. 1–26, 2022.
- [4] Weiyang Chen, Kai Niu, Deng Zhao, Rong Zheng, Dan Wu, Wei Wang, Leye Wang, and Daqing Zhang, “Robust dynamic hand gesture interaction using lte terminals,” in *2020 19th ACM/IEEE International Conference on Information Processing in Sensor Networks (IPSN)*. IEEE Computer Society, 2020, pp. 109–120.
- [5] Wenwei Li, Ruiyang Gao, Jie Xiong, Jiarun Zhou, Leye Wang, Xingjian Mao, Enze Yi, and Daqing Zhang, “Wifi-csi difference paradigm: Achieving efficient doppler speed estimation for passive tracking,” *Proceedings of the ACM on Interactive, Mobile, Wearable and Ubiquitous Technologies*, vol. 8, no. 2, pp. 1–29, 2024.
- [6] Fusang Zhang, Zhaoxin Chang, Kai Niu, Jie Xiong, Beihong Jin, Qin Lv, and Daqing Zhang, “Exploring lora for long-range through-wall sensing,” *Proceedings of the ACM on Interactive, Mobile, Wearable and Ubiquitous Technologies*, vol. 4, no. 2, pp. 1–27, 2020.
- [7] Manikanta Kotaru, Kiran Joshi, Dinesh Bharadia, and Sachin Katti, “Spotfi: Decimeter level localization using wifi,” in *Proceedings of the 2015 ACM conference on special interest group on data communication*, 2015, pp. 269–282.
- [8] Deepak Vasisht, Swarun Kumar, and Dina Katabi, “{Decimeter-Level} localization with a single {WiFi} access point,” in *13th USENIX symposium on networked systems design and implementation (NSDI 16)*, 2016, pp. 165–178.
- [9] Dan Wu, Ruiyang Gao, Youwei Zeng, Jinyi Liu, Leye Wang, Tao Gu, and Daqing Zhang, “Fingerdraw: Sub-wavelength level finger motion tracking with wifi signals,” *Proc. ACM Interact. Mob. Wearable Ubiquitous Technol.*, vol. 1, no. 1, 2020.
- [10] Xiang Li, Shengjie Li, Daqing Zhang, Jie Xiong, Yasha Wang, and Hong Mei, “Dynamic-music: accurate device-free indoor localization,” in *Proceedings of the 2016 ACM International Joint Conference on Pervasive and Ubiquitous Computing*. ACM, 2016, pp. 196–207.
- [11] Chen Chen, Yan Chen, Hung-Quoc Lai, Yi Han, and KJ Ray Liu, “High accuracy indoor localization: A wifi-based approach,” in *2016 IEEE international conference on acoustics, speech and signal processing (ICASSP)*. IEEE, 2016, pp. 6245–6249.
- [12] Jincao Zhu, Youngbin Im, Shivakant Mishra, and Sangtae Ha, “Calibrating time-variant, device-specific phase noise for cots wifi devices,” in *Proceedings of the 15th ACM Conference on Embedded Network Sensor Systems*, 2017, pp. 1–12.
- [13] Nan Yu, Wei Wang, Alex X Liu, and Lingtao Kong, “Qgesture: Quantifying gesture distance and direction with wifi signals,” *Proceedings of the ACM on Interactive, Mobile, Wearable and Ubiquitous Technologies*, vol. 2, no. 1, pp. 1–23, 2018.
- [14] Kun Qian, Chenshu Wu, Zimu Zhou, Yue Zheng, Zheng Yang, and Yunhao Liu, “Inferring motion direction using commodity wi-fi for interactive exergames,” in *Proceedings of the 2017 CHI conference on human factors in computing systems*, 2017, pp. 1961–1972.
- [15] Xiang Li, Daqing Zhang, Qin Lv, Jie Xiong, Shengjie Li, Yue Zhang, and Hong Mei, “Indotrack: Device-free indoor human tracking with commodity wi-fi,” *Proceedings of the ACM on Interactive, Mobile, Wearable and Ubiquitous Technologies*, vol. 1, no. 3, pp. 72, 2017.
- [16] Kun Qian, Chenshu Wu, Yi Zhang, Guidong Zhang, Zheng Yang, and Yunhao Liu, “Widar2. 0: Passive human tracking with a single wi-fi link,” in *Proceedings of the 16th Annual International Conference on Mobile Systems, Applications, and Services*, 2018, pp. 350–361.
- [17] Youwei Zeng, Dan Wu, Ruiyang Gao, Tao Gu, and Daqing Zhang, “Fullbreathe: Full human respiration detection exploiting complementarity of csi phase and amplitude of wifi signals,” *Proceedings of the ACM on Interactive, Mobile, Wearable and Ubiquitous Technologies*, vol. 2, no. 3, pp. 148, 2018.
- [18] Xinyu Li, J Andrew Zhang, Kai Wu, Yuanhao Cui, and Xiaojun Jing, “Csi-ratio-based doppler frequency estimation in integrated sensing and communications,” *IEEE sensors journal*, vol. 22, no. 21, pp. 20886–20895, 2022.
- [19] Yanmo Hu, Kai Wu, J Andrew Zhang, Weibo Deng, and Y Jay Guo, “Performance bounds and optimization for csi-ratio based bi-static doppler sensing in isac systems,” *IEEE Transactions on Wireless Communications*, 2024.
- [20] Zhitong Ni, J Andrew Zhang, Kai Wu, and Ren Ping Liu, “Up-link sensing using csi ratio in perceptive mobile networks,” *IEEE Transactions on Signal Processing*, vol. 71, pp. 2699–2712, 2023.
- [21] Dan Wu, Youwei Zeng, Ruiyang Gao, Shenjie Li, Yang Li, Rahul C Shah, Hong Lu, and Daqing Zhang, “Witraj: Robust indoor motion tracking with wifi signals,” *IEEE Transactions on Mobile Computing*, vol. 22, no. 5, pp. 3062–3078, 2021.
- [22] Tristan Needham, *Visual complex analysis*, Oxford University Press, 2023.
- [23] Daniel Halperin, Wenjun Hu, Anmol Sheth, and David Wetherall, “Tool release: gathering 802.11 n traces with channel state information,” *ACM SIGCOMM Computer Communication Review*, vol. 41, no. 1, pp. 53–53, 2011.